UNIVERSITY
OF WOLLONGONG
AUSTRALIA

University of Wollongong
Research Online

Faculty of Engineering and Information Sciences - Papers: Part A

Faculty of Engineering and Information Sciences

2017

A 3D lateral electrode structure for diamond based microdosimetry

Jeremy A. Davis
University of Wollongong, jeremyd@uow.edu.au

Kumaravelu Ganesan
University of Melbourne

Dale A. Prokopovich
University of Wollongong, dalep@uow.edu.au

Marco Petasecca
University of Wollongong, marcop@uow.edu.au

Michael L. F Lerch
University of Wollongong, mlerch@uow.edu.au

See next page for additional authors

Publication Details

Davis, J. A., Ganesan, K., Prokopovich, D. A., Petasecca, M., Lerch, M. L. F., Jamieson, D. N. & Rosenfeld, A. B. (2017). A 3D lateral electrode structure for diamond based microdosimetry. Applied Physics Letters, 110 (1), 013503-1-013503-4.

Research Online is the open access institutional repository for the University of Wollongong. For further information contact the UOW Library: research-pubs@uow.edu.au

A 3D lateral electrode structure for diamond based microdosimetry

Abstract
A diamond based microdosimeter prototype featuring a 3D lateral electrode structure was created using laser ablation and active brazing alloys and characterised by means of ion beam induced charge collection measurements and finite element analysis, using Synopsys TCAD simulation package.

Keywords
diamond, microdosimetry, structure, lateral, electrode, 3d

Disciplines
Engineering | Science and Technology Studies

Publication Details
Davis, J. A., Ganesan, K., Prokopovich, D. A., Petasecca, M., Lerch, M. L. F., Jamieson, D. N. & Rosenfeld, A. B. (2017). A 3D lateral electrode structure for diamond based microdosimetry. Applied Physics Letters, 110 (1), 013503-1-013503-4.

Authors
Jeremy A. Davis, Kumaravelu Ganesan, Dale A. Prokopovich, Marco Petasecca, Michael L. F Lerch, David Jamieson, and Anatoly B. Rosenfeld

This journal article is available at Research Online: http://ro.uow.edu.au/eispapers/6311

A 3D lateral electrode structure for diamond based microdosimetry

Jeremy A. Davis,[1,a) b) c)] Kumaravelu Ganesan,[2,b)] Dale A. Prokopovich,[3,c)]
Marco Petasecca,[1] Michael L. F. Lerch,[1] David N. Jamieson,[2] and Anatoly B. Rosenfeld[1]
[1]*Centre for Medical Radiation Physics, University of Wollongong, Wollongong, 2500 NSW, Australia*
[2]*School of Physics, University of Melbourne, Parkville, 3052 VIC, Australia*
[3]*Australian Nuclear Science and Technology Organisation, Lucas Heights, 2234 NSW, Australia*

(Received 20 June 2016; accepted 22 December 2016; published online 6 January 2017)

A diamond based microdosimeter prototype featuring a 3D lateral electrode structure was created using laser ablation and active brazing alloys and characterised by means of ion beam induced charge collection measurements and finite element analysis, using Synopsys TCAD simulation package. *Published by AIP Publishing*. [http://dx.doi.org/10.1063/1.4973628]

Diamond has been identified as a desirable material for use in dosimetry due to its near tissue equivalence and radiation hardness.[1,2] A previous study identified that a correction factor based upon stopping power ratios ($\frac{S_D}{S_W}$) could be used to convert the energy deposition in diamond to water for protons and alpha particles with an energy range between 1 MeV and 10 GeV.[3] Furthermore, a number of studies support the use of diamond as a dosimetric material in clinical applications for photons,[4,5] given the well known signal dependence on the atomic composition (Z). Diamond has been shown to exhibit energy independence for photon beams (6–15 MV) and for electron beams (6–20 MeV).[6,7] This result is obvious, given the relative equality in the atomic number of carbon ($Z = 6$) and of tissue ($Z = 7.4$). This equality leads to a constant mass attenuation coefficient and mass stopping power ratios for photons and electrons, respectively, over a given energy regime of interest for radiotherapy.[8,9]

A core feature of diamond based radiation detectors is their simplistic design, which allows for versatility in the structures which may be produced, without the need for p-n junctions. In addition to this, their radiation hardness and tissue equivalence make them desirable for microdosimetric applications in harsh radiation environments. At the Centre for Medical Radiation Physics (CMRP), the primary aim in the development of diamond based radiation detectors has been the investigation and comparison of alternative fabrication methods for creating isolated micron sized 3D Sensitive Volumes (SV) for the purpose of microdosimetry.[10] While previous work in diamond microdosimetry has primarily been devoted to planar structures,[11] the work presented in this paper investigates the viability of current fabrication technologies in creating lateral structures. The long term aim of such work is to create devices similar in function to those currently developed in silicon-on-insulator such as the 3D-MESA Bridge microdosimeter.[12]

Here, we present a diamond microdosimeter/radiation detector prototype featuring a lateral electric field structure, created by using a combination of selective laser ablation and active brazing alloys. The 3D Lateral Electrode Structure (3D-LES) device utilised in this study was fabricated at the University of Melbourne in ultra high purity type IIa single crystal diamond sourced from Element 6.[13] Laser ablation milling, using an Oxford alpha series laser was used to fabricate isolation trenches and wells for contact electrodes. Electrode wells were created in pairs with dimensions of $80 \times 60 \times 30\ \mu m^3$ (see Fig. 1) separated by 10, 20, and 30 μm. The wells were braised with a silver active brazing alloy and biased to produce a lateral electric field in the sensitive volume between the electrodes. In some devices, isolation trenches (width = 5 μm and depth = 60 μm) were then created using further laser ablation ($160 \times 300\ \mu m^2$), to surround the contact electrodes, thereby reducing charge collection from outlying regions. The walls of the isolation trench retain a thin conducting layer[14] arising from the laser ablation process. The surface of the device is then polished with a Struers Rotopol system to remove any remaining braise alloy from the surface. Optical profilometry and probe testing were performed to ensure all the surface metal has been removed. The devices were then mounted upon a ceramic carrier and wire bonded to allow for experimental characterisation. Measurements on all devices revealed consistent and reproducible characteristics. Presented here are representative measurements on two devices: device D2 (contact separation = 20 μm, with isolation trench) and device D4 (contact separation = 10 μm, without isolation trench).

The current-voltage (IV) characteristics of the devices were tested using a Keithley 6517A electrometer, over a bias range of $-50 < V < 50$ in 1 V increments with time delay of 2 s between measurements for stabilisation. The minimum current threshold was set to 1 μA. The analysis of the IV curves presented in Fig. 2 allows for a determination of the breakdown behaviour for each device. It can be seen that the optimal bias conditions for both devices is approximately $-40 < V < 40$. Given the contact separation for D4 (10 μm), this corresponds to electric field strengths up to 4 V μm^{-1}, and likewise for D2 (20 μm). The IV characteristics of D2 (contact separation = 20 μm, with isolation trench) show a counter-intuitive increased magnitude of current per applied bias, compared with D4 (contact separation = 10 μm, without isolation trench). In device D2, the conducting walls of the

[a)]Author to whom correspondence should be addressed. Electronic mail: jeremyd@uow.edu.au
[b)]J. A. Davis and K. Ganesan contributed equally to the fabrication of the device presented in this paper.
[c)]J. A. Davis and D. A. Prokopovich contributed equally to the experimental characterisation of the device presented in this paper.

RIGHTSLINK

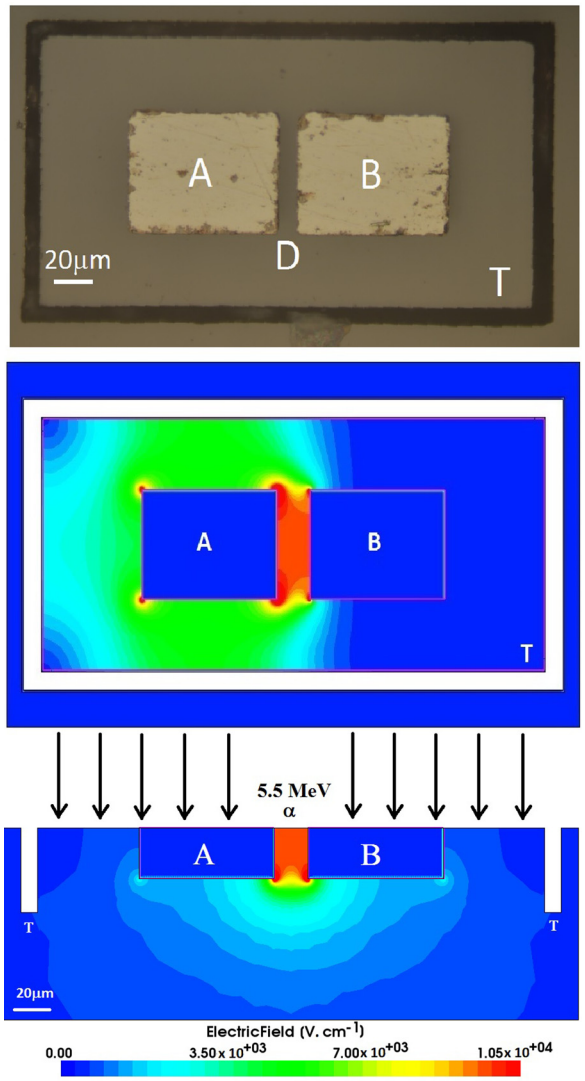

FIG. 1. (Upper) Top view optical image of a representative device before wire bonding showing: A,B contact electrodes, T isolation trench, and D contact separation distance. (Middle) Top view simulation of the electric field distribution, with graphite coated trench modelled. (Lower) Cross sectional view, without graphite coated trench modelled. The simulations depict the electric field due to a potential difference between adjacent electrodes of 20 V with a substrate thickness of 500 μm. The vertical scale is compressed in the lower image, and the arrow indicates the range of 5.5 MeV He^{2+} ions used in charge collection study. The experimental devices have contact separations of 10, 20, and 30 μm.

isolation trench act like a virtual electrode, with surface charge leading to a difference in potential compared with the biased electrode, thus creating an additional electric field component and higher leakage current. The capacitance of each device was measured over a bias range of $0 < V < 20$ at 1.2 pE, using Boonton capacitance meter (Model 7200) controlled by a Personal Computer (PC) via an IEEE-488 interface. The small capacitance measured is consistent with the small size of device volumes and of materials with low dielectric constant (i.e., diamond $\epsilon \approx 5.6$).

To interpret the experimental results, a 2D model of device D2 was developed using Synopsys Technology Computer Aided Design (TCAD).[15] The Device Simulation for Smart Integrated Systems (DESSIS) simulation package was used to characterise the electrical and charge collection behaviour under experimental conditions. Since at this point

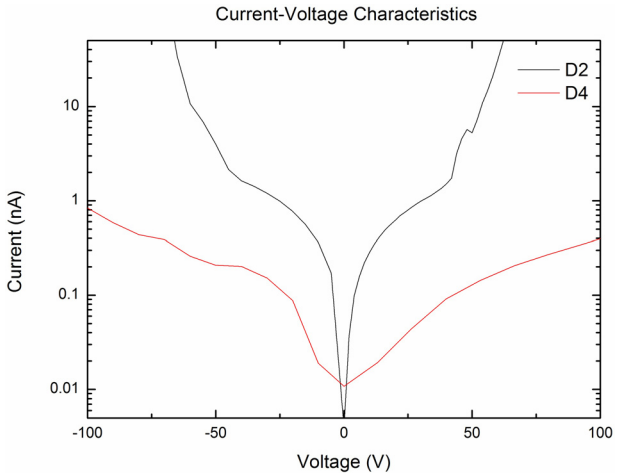

FIG. 2. Experimental IV characteristics of 3D-LES device. IV curves for two devices D2 and D4 are shown.

in time, diamond is not a standard material within the Synopsys material database, the diamond bulk was modelled as an insulator with material properties (dielectric constant, resistivity, band-gap, and charge mobilities) adjusted to represent diamond. This model is sufficient for the needs of this work, simply to solve the Laplace and Poission equations for field structure within diamond. Fig. 1 depicts the results which coincide with 20 V, applied to electrode A (contact separation = 20 μm). This bias condition was chosen specifically to give an electric field strength between the two electrodes of 1 μm^{-1}. A consistently uniform lateral electric field is produced between the two electrodes, as expected. In addition, the electric field is shown to extend well below the electrodes, thereby increasing the volume of the sensitive volume and potentially leading to undesirable degradation of the spatial resolution.

Although the thickness of the diamond substrate does not have direct effect upon electric field in the SV, as is the case with top-down metal-insulator-metal designs, reduction in the substrate thickness is still necessary to reduce the sensitive volume and improve the spatial resolution. To examine the effect of separation distance, the electric field strength versus depth was plotted, along the medial line of the SV. This simulation study was performed for three devices having respective inter-contact distances of 10, 20, and 30 μm. The bias conditions were set at 10, 20, and 30 V for the three devices, respectively, to obtain equivalent electric field strength between adjacent electrodes. The result as presented in Fig. 3 demonstrates the expected role of the contact electrode separation distance and electric field profile on the sensitive volume.

To ascertain the effectiveness of the 3D-LES design for microdosimetric purposes, Ion Beam Induced Charge (IBIC) measurements[16] were undertaken. These measurements were performed upon the Heavy Ion Microprobe beam line of the ANTARES 10 MV tandem accelerator at the Australian Nuclear Science and Technology Organisation (ANSTO). The IBIC study was performed using 5.5 MeV He^{2+} ions, having a range in diamond and silver of 13.62 and 11.67 μm, respectively.[17] Ion beam current during the experiment was low (approximately 100 ± 10 ions s^{-1}) so that signals from

RIGHTSLINK

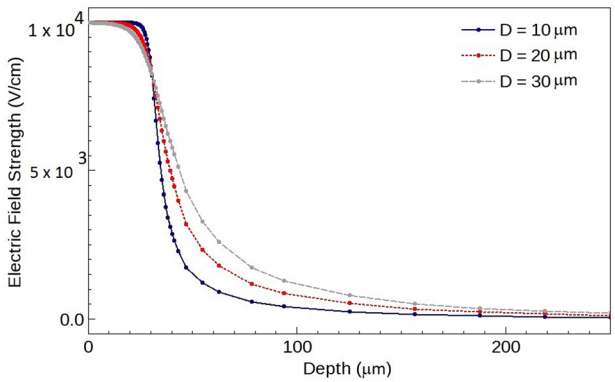

FIG. 3. Electric field strength versus depth in substrate along the medial line of the SV (see Fig. 1).

individual ion impacts could be acquired consistent with the time constant of the data acquisition system. The ions were incident normal to the diamond, focussed to approximately 1–2 μm spot size resolution[18] and raster scanned across the device. The positive bias was applied to electrode A, while electrode B was connected to a virtual ground (see Fig. 1 for electrode configuration). The signal due to induced charge carriers (electrons) was collected from the biased contact (A), via a charge sensitive preamplifier (Amptek A250), a shaping amplifier, and a multi-channel analyzer. The generated signal has an amplitude equivalent to the ionisation energy induced by each ion impact and was recorded along with beam position to form data triplets (x, y, energy). Energy calibration was then performed using a pulse generator calibrated with a 300 μm thick windowless silicon PIN diode with known Charge Collection Efficiency (CCE) of 100% and allowing for the energies required to create an electron hole pair in silicon (3.6 eV) compared to diamond (13.2 eV). Median energy maps for devices D4 and D2 are shown in Fig. 4 with their corresponding energy spectra. The peak in the energy spectrum situated at 5.4 MeV corresponds to a CCE of 98%, and is associated with the sensitive volume between the two electrodes, where the electric field is highest. The rest of the charge collection spectrum portrays a broad continuum form of the diminishing electric field with the lateral distance away from the sensitive volume. In device D2, which differs from device D4 by the inclusion of a boundary trench, an additional peak is evident in the energy spectrum at 2.1 MeV, corresponding to 38% CCE

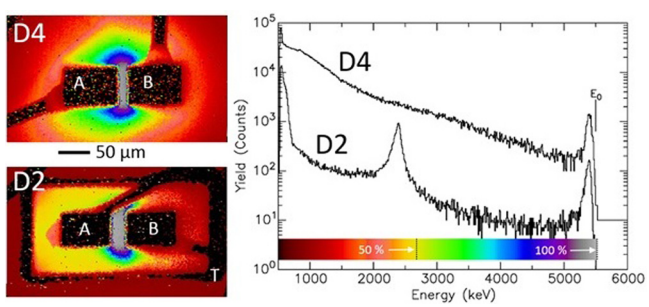

FIG. 4. (Left) IBIC median energy maps of devices D4 (electrode separation = 10 μm, bias = 10 V and no boundary trench) and D2 (electrode separation = 20 μm, bias = 20 V, includes boundary trench). (Right) Corresponding total energy spectra from each device with the colour scale applicable to the median energy maps. E_0 designates the beam energy.

which is due to signals generated from the device outside the sensitive volume but within the isolation trench, as seen in the map. This peak arises from the electric fields generated by the potential between the electrodes and the conductive graphitic material remaining in the isolation trench. These fields may be explained by the method of images, whereby the presence of free charge carriers between the electrode and boundary trench induces surface charge of equal and opposite magnitude, creating an additional field component that would be qualitatively similar to what is depicted in the model shown in Fig. 1. A comparison of Fig. 1 with the median energy map in Fig. 4 for device D2 shows how this electric field can explain the magnitude of the charge collection efficiency in the volume between the isolation trench walls and the collecting electrode.

The devices also show sustained high charge collection efficiency as a function of contact electrode spacing that also varies the sensitive volume. Shown in Fig. 5 are representative IBIC median energy maps for devices similar to D4 (without isolation trench) for contact electrode spacings of 10, 20, and 30 μm. Small variations in the energy peak position for signals extracted from just the sensitive volume between the electrodes (also shown in Fig. 5) arise from small fabrication variations but show strong consistency of high charge collection efficiency. These results show that our method of fabricating prototype diamond microdosimeters is viable. Laser ablation of diamond in conjunction with silver brazing metal, used to fabricate devices in high purity electronic grade type IIa single crystal synthetic diamond from Element 6,[13] results in devices with close to 100% charge collection efficiency, which is sustained over varying sensitive volumes.

As with previous studies, the boundary trench plays a role in confining charge collection to within the bounded region for 5.5 MeV He^{2+} ions.[11] This result is promising as a proof of concept; however, it needs to be noted that the range of charged particles is less than that of the trench depth. As such, an increase in particle range would lead to undesirable expansion of the sensitive volume and thus reduced

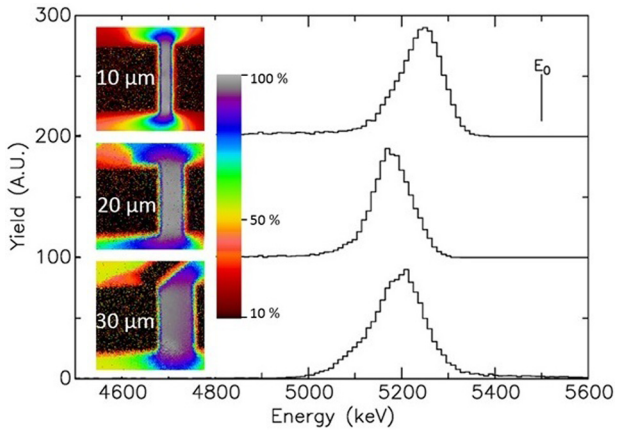

FIG. 5. IBIC energy spectra from the sensitive volume of devices similar to D2 (without isolation trench) and (inset) corresponding median energy maps for devices with 10 μm (top), 20 μm (middle), and 30 μm (bottom) separation. The energy spectra were extracted from just the area of the device between the contract electrodes; E_0 designates the beam energy and the colour scale shows the charge collection efficiency.

RIGHTSLINK

confinement. One solution would involve matching the trench depth to the substrate thickness. The ideal case, however, would be to completely separate individual devices from the surrounding substrate, as well as replacing the ablated diamond with a tissue equivalent medium (i.e., PMMA), for the purpose of creating physically isolated structures. However, in order to mitigate the effects of graphitic residue, improvements will need to be implemented in either the method of ablation and removal of the residual conducting layer. Use of a thinned substrate would also further limit charge collection from underneath the contact electrodes. An alternative approach could be the growth of a thin layer of detector grade diamond upon a low quality diamond substrate, separated by a layer of insulating polycrystalline diamond. This technique would limit charge sharing from the substrate without sacrificing mechanical strength.

The TCAD models have shown the importance of the electrode geometry to define the sensitive volume of material between the electrodes. As expected, the sensitive volume scales down with decreasing electrode spacing. The experimental data presented here on these prototype devices constructed from electronic grade synthetic diamond show the remarkably high charge collection efficiency possible from the high quality diamond material and also the validity of the numerical models. This suggests that electronic grade diamond offers many advantages for radiation detectors in many applications in addition to radiation dosimetry, including detectors for high energy physics experiments or adverse radiation environments wherever radiation hardness, fast detection, and large charge collection distances and efficiency are required.

The authors would like to acknowledge the efforts of the Accelerator Operations Team, Institute of Environmental Research (IER), ANSTO. This project was partially supported by the Australian Research Council (ARC) Grant No. DP 1096600.

[1]S. Almaviva, M. Marinelli, E. Milani, G. Prestopino, A. Tucciarone, C. Verona, G. Verona-Rinati, M. Angelone, M. Pillon, I. Dolbnya, K. Sawhney, and N. Tartoni, J. Appl. Phys. **107**, 1 (2010).
[2]S. Lagomarsino, M. Bellini, C. Corsi, V. Cindro, K. Kanxheri, A. Morozzi, D. Passeri, L. Servoli, C. J. Schmidt, and S. Sciortino, Appl. Phys. Lett. **106**, 193509 (2015).
[3]J. A. Davis, S. Guatelli, M. Petasecca, M. L. F. Lerch, M. I. Reinhard, M. Zaider, J. Ziegler, and A. B. Rosenfeld, IEEE Trans. Nucl. Sci. **61**, 1544 (2014).
[4]P. W. Hoban, M. Heydarian, W. A. Beckham, and A. H. Beddoe, Phys. Med. Biol. **39**, 1219 (1994).
[5]G. T. Betzel, S. P. Lansley, F. Baluti, L. Reinisch, and J. Meyer, Phys. Med. **28**, 144 (2012).
[6]W. U. Laub, T. W. Kaulich, and F. Nüsslin, Med. Phys. **24**, 535 (1997).
[7]W. U. Laub and R. Crilly, J. Appl. Clin. Med. Phys. **15**, 92 (2014).
[8]M. Berger, J. Coursey, M. Zucker, and J. Change, *ESTAR, PSTAR, and ASTAR: Computer Programs for Calculating Stopping-Power and Range Tables for Electrons, Protons, and Helium Ions (Version 1.2.3)* (National Institute of Standards and Technology, 2005).
[9]H. Bouchard, Y. Kamio, H. Palmans, J. Seuntjens, and S. Duane, Med. Phys. **42**, 6033 (2015).
[10]A. B. Rosenfeld, Nucl. Instrum. Methods Phys. Res., Sect. A **809**, 156 (2016).
[11]J. A. Davis, K. Ganesan, A. D. C. Alves, D. A. Prokopovich, S. Guatelli, M. Petasecca, M. L. F. Lerch, D. N. Jamieson, and A. B. Rosenfeld, IEEE Trans. Nucl. Sci. **61**, 3479 (2014).
[12]L. T. Tran, L. Chartier, D. A. Prokopovich, M. I. Reinhard, M. Petasecca, S. Guatelli, M. L. F. Lerch, V. L. Perevertaylo, M. Zaider, N. Matsufuji, M. Jackson, M. Nancarrow, and A. B. Rosenfeld, IEEE Trans. Nucl. Sci. **62**, 504 (2015).
[13]See http://www.e6.com/ for the website of the manufacturer, Element 6: Synthetic Industrial Diamonds.
[14]N. H. Rizvi, Laser Precis. Manuf. **50**, 1 (2003).
[15]Synopsys SENTAURUS TCAD I-2013.12, see https://www.synopsys.com/silicon/tcad.html.
[16]M. B. H. Breese, J. Appl. Phys. **74**, 3789 (1993).
[17]J. F. Ziegler, M. D. Ziegler, and J. P. Biersack, Nucl. Instrum. Methods Phys. Res., Sect. B **268**, 1818 (2010).
[18]R. Siegele, A. G. Kachenko, M. Ionescu, and D. D. Cohen, Nucl. Instrum. Methods Phys. Res., Sect. B **267**, 2054 (2009).

RIGHTSLINK